Published in final edited form as:
J Cereb Blood Flow Metab. 2004 March ; 24(3): 280–290.

Effects of Reperfusion on ADC and CBF Pixel-by-Pixel Dynamics in Stroke: Characterizing Tissue Fates using Quantitative Diffusion and Perfusion Imaging

Qiang Shen[*,†], **Marc Fisher**[‡,§], **Christopher H. Sotak**[‖,§], and **Timothy Q. Duong**[*,†]

[*]Center for Comparative NeuroImaging, University of Massachusetts Medical Center, Worcester, MA, USA

[†]Department of Psychiatry, University of Massachusetts Medical Center, Worcester, MA, USA

[‡]Department of Neurology, University of Massachusetts Medical Center, Worcester, MA, USA

[§]Department of Radiology, University of Massachusetts Medical Center, Worcester, MA, USA

[‖]Departments of Biomedical Engineering and Chemistry & Biochemistry, Worcester Polytechnic Institute, Worcester, MA, USA

Summary

The effects of reperfusion on the spatiotemporal dynamics of transient (60 minutes) focal ischemic brain injury in rats were evaluated *on a pixel-by-pixel basis* using quantitative cerebral blood flow (CBF) and apparent diffusion coefficient (ADC) measurements every 30 minutes for 3 hours and compared to post-mortem histology at 24 hours. Four biologically relevant clusters were classified based on ADC ($0.53 \pm 0.02 \times 10^{-3}$mm^2/s, SD) and CBF (0.30 ± 0.09ml/g/min) viability thresholds, namely: (1) the "normal" cluster with ADC and CBF > thresholds; (2) the "mismatch" cluster with ADC > threshold but CBF < threshold; (3) the "core" cluster with ADC and CBF < thresholds; and (4) "non-nourishing reperfusion zone" where ADC < threshold but CBF > threshold. The spatio-temporal progression of tissue volumes, ADC and CBF of each cluster were evaluated. Pixels of each cluster on the CBF-ADC space were mapped onto the image space. Following reperfusion, 28% of the "core" pixels and 90% of the "mismatch" (defined at 60 minutes) pixels were salvaged at 180 minutes, which correlated with histology. The ADC and CBF of subsequently salvaged tissues were significantly higher than those became infarcted. Salvaging "core" pixels indicated that reduced ADC was not synonymous with irreversible injury; duration of exposure and severity of reduced ADC and CBF were likely critical. Projection profiles showed a bimodal ADC, but uni-modal CBF, distributions. The ADC bimodal minima, obtained without histological correlation, were similar to the histology-derived ADC and CBF viability thresholds, and could have potential clinical applications. This study demonstrated a simple but powerful approach to evaluate, on a pixel-by-pixel basis, the spatio-temporal evolution of ischemic brain injury, and a potential for statistical prediction of tissue fate.

Keywords

Penumbra; Oligemia; Viability thresholds; Hyperemia; Perfusion-diffusion mismatch; Stroke; DWI; PWI

Address correspondence and reprint requests to Timothy Q Duong, PhD, Center for Comparative NeuroImaging, University of Massachusetts Med Sch, 55 Lake Ave N, Worcester, MA 01655, USA; timothy.duong@umassmed.edu.

Introduction

Spin-density, T_1, and T_2 imaging abnormalities appear to indicate predominantly irreversible ischemic brain injury (Moseley et al., 1990; Fisher and Albers, 1999). Magnetic resonance diffusion-weighted imaging (DWI) is capable of mapping reversible and irreversible injury and is widely recognized as a powerful tool for early detection and evaluation of stroke in both animal models and humans (Moseley et al., 1990; Fisher and Albers, 1999). Hyperintense regions on DWI correspond to tissues with reduced apparent diffusion coefficient (ADC) of water. Similarly, magnetic resonance perfusion-weighted images (PWI), which provide an index of cerebral blood flow (CBF), are useful in detecting perfusion deficits associated with ischemic injury. Quantitative perfusion and diffusion imaging could yield a finer discrimination of tissue status based on their intrinsic diffusion and perfusion characteristics, potentially offering a means for statistical prediction of tissue fate (Zhao et al., 1997; Franke et al., 2000; Wu et al., 2001).

Data from experimental stroke models and stroke patients have demonstrated that there is usually a gradual progression of potentially reversible cerebral ischemic injury towards infarction. A central core with severely compromised CBF is surrounded by a rim of moderately ischemic tissue with diminished CBF and impaired electrical activity but preserved cellular metabolism, commonly known as the “ischemic penumbra” (Astrup et al., 1981). The penumbra is the region at risk of eventual infarction and is of most interest for potential therapy. It has been postulated that the “perfusion-diffusion mismatch” seen initially after stroke onset approximates the “ischemic penumbra.” Lesion volumes based on PWI are generally larger than those based on DWI at early time points and this mismatch becomes smaller over time (Baird et al., 1997; Karonen et al., 1999; Neumann et al., 1999). Although a strict definition of the ischemic penumbra requires correlation with energy metabolism (Back et al., 1994; Hoehn-Berlage et al., 1995; Kohno et al., 1995) and such correlation is not feasible in humans, the “ischemic penumbra” has been operationally defined using DWI, PWI or equivalent modalities (Kaufmann et al., 1999; Schlaug et al., 1999). Furthermore, studies in humans (Baird et al., 1997; Karonen et al., 1999; Neumann et al., 1999) have shown that part of the ischemic lesions could be salvaged by therapeutic intervention. For example, thrombolytic therapy has been shown to be effective in salvaging some tissues within 3 hours after stroke onset (Kidwell et al., 2000). To help expand the time window for thrombolytic therapy and identify patient candidates for treatment, it would be beneficial to have the means to identify “tissue signature” and a “clock window” in order to achieve maximum benefit and avoid devastating intraparenchymal hemorrhage (Albers, 1999).

Although the “perfusion-diffusion mismatch” is widely observed in acute human stroke (Albers, 1999; Schlaug et al., 1999; Rohl et al., 2001), similar observations in animal stroke models (Lythgoe et al., 1999; Carano et al., 2000) have been limited and the temporal evolution of the perfusion-diffusion mismatch in animal models has yet to be systematically investigated. Further, most studies used region-of-interest analysis, instead of pixel-by-pixel analysis to resolve tissue fates in the acute phase as they evolved in the image and CBF-ADC spaces.

In this study, we utilized quantitative perfusion and diffusion imaging at reasonably high spatiotemporal resolution to investigate, on a pixel-by-pixel basis, the effects of reperfusion in transient focal ischemia in rats during the acute phase. The main goals were: (1) to evaluate the pixel-by-pixel temporal and spatial dynamics of the ADC- and CBF-derived lesion volumes in transient ischemic injury; (2) to map different pixel clusters on the CBF–ADC space to the image space; and (3) to characterize the ADC and CBF values of pixels that were subsequently salvaged by reperfusion and those that subsequently became infarcted.

Materials and Methods

Animal preparations

Stroke surgery and the anesthetic protocol were identical to those of Li et al. (Li et al., 1999) and are briefly described below. Six male Sprague-Dawley rats (300 to 350g, Taconic Farms, NY, USA) were initially anesthetized with choral hydrate (400 mg/kg, i.p., Sigma, St. Louis, USA). The right femoral artery was catheterized for blood-gas sampling, continuous blood-pressure and heart-rate monitoring. Transient focal brain ischemia of the right hemisphere was induced using the intraluminal middle cerebral artery occlusion (MCAO) method; reperfusion was performed at 60 minutes post-occlusion by remotely withdrawing the occluder while the animals were in the magnet (the occluder stayed in the internal carotid artery close to the external carotid artery bifurcation after reperfusion). Rectal temperature was maintained at 36.5 to 37.5° C throughout. Blood pressure, heart rate and respiration rate (derived via the slower modulation on top of the cardiac waveforms) were recorded continuously onto a PC via the Biopac system (Santa Barbara, CA, USA). Anesthesia was switched to 1% isoflurane once the animal was in the magnet and during imaging. MRI data were acquired at 30, 60, immediately after reperfusion (labeled as 70 minute), 90, 120, 180 minutes, and 24 hours post-occlusion, followed immediately by TTC (2,3,5-triphenyltetrazolium chloride) staining. Brief comparisons were also made with a group of permanent occlusion animals described previously (n = 11) (Shen et al., 2003). Stroke surgery, experimental conditions, imaging experiments, and data analysis were the same as those of the reperfusion group.

Histology

TTC staining was performed at 24 hours post-ischemia. Seven 1.5-mm slices corresponding to the MRI slices were carefully sectioned coronally and incubated in 2% solution of TTC at 37° C for 30 minutes and fixed in 10% buffered formalin solution. Brain slices were photographed using a CCD camera and analyzed using image-analysis software (BioScan OPTIMAS, Edmonds, WA, USA). The stained regions were defined as normal and the unstained regions were defined as infracted lesions. To compensate for edema, a swelling factor was determined by subtracting the total volume of the normal hemisphere from the ischemic hemisphere (Tatlisumak et al., 1998). The edema-corrected lesion volume was obtained by subtracting the swelling volume from the ischemic volume.

MR experiments

MRI was performed on a Bruker 4.7-T/40-cm (Billerica, MA, USA) and a 20-G/cm gradient insert (ID = 12 cm, 120-μs rise time). The animal was placed into a stereotaxic headset and onto an animal holder, which consisted of an actively-decoupled surface coil (2.3-cm ID) for brain imaging and a neck coil for CBF labeling. Coil-to-coil interaction was actively decoupled.

ADC_{av} was obtained by averaging three ADC maps acquired separately with diffusion-sensitive gradients applied along the x, y or z direction (Stejskal and Tanner, 1965). ADC_{av} was used because it yielded a single ADC value, which minimized structural anisotropy (Lythgoe et al., 1997). Single-shot, spin-echo, echo-planar images (EPI) were acquired with TR = 2 seconds (90° flip angle), matrix = 64 × 64, FOV = 2.5 cm × 1.9 cm, seven 1.5-mm slices, TE = 43 milliseconds, b = 10 and 1504 s/mm^2, Δ = 20 milliseconds, δ = 6.5 milliseconds, and 16 averages (total time = 128 seconds).

Quantitative CBF was measured using the continuous arterial spin-labeling technique (Williams et al., 1992; Silva et al., 1999) with single-shot, gradient-echo EPI. Paired images were acquired alternately—one with arterial spin-labeling and the other without spin-labeling (control) preparation. The MRI parameters were: TE = 15 milliseconds, TR = 2 seconds (90° flip angle), matrix = 64 × 64, FOV = 2.5 cm × 1.9 cm, and seven 1.5-mm slices. The continuous

arterial spin labeling employed a 1.78-second square radiofrequency pulse to the labeling coil in the presence of 1.0 G/cm gradient. The sign of the frequency offset was switched for non-labeled images. For each set of CBF measurement, 100 pairs of images were acquired for signal averaging (total times = 6.7 minutes) – with 50 pairs were acquired before and 50 pairs after the ADC_{av} measurement. Although differences in dephasing effects between spin-echo and gradient-echo EPI could cause pixel misalignment at the skull-brain interface, it was minimized by using a short gradient echo time, similar EPI readout time, and careful shimming. Further, a conservative ROI avoiding the brain-skull interface was used for data analysis.

Data analysis

MR data analysis employed code written in Matlab (Math-Works, Natick, MA, USA) and STIMULATE software (Strupp, 1996). Analysis was performed on conservative ROIs, which were carefully drawn to avoid the edge of the brain-skull interface based on CBF maps with reference to ADC maps to verify alignment.

Calculation of ADC and CBF maps

ADC maps with intensity in unit of mm^2/s were calculated pixel-by-pixel by using (Stejskal and Tanner, 1965),

$$ADC = -\ln(S_i/S_o)/(b_i - b_o).$$

where $b_i = \gamma^2 G_i^2 \delta^2 (\Delta - \delta/3)$, ln is the natural logarithm, S_1 is the signal intensity obtained with b_i, and S_o is the signal intensity obtained with b_o. The b-value is proportional to the gradient strength (G), magnetogyric ratio (γ), duration of each gradient pulse (δ), and the time between application of the two gradient pulses (Δ).

CBF images (S_{CBF}) with intensity in units of ml per gram tissue per minute (ml/g/min) were calculated pixel-by-pixel using (Silva et al., 1997b),

$$S_{CBF} = \lambda/T_1 \times (S_C - S_L)/(S_L + (2\alpha - 1)S_C).$$

where S_C and S_L are signal intensities of the control and labeled images, respectively. λ is the water brain-blood partition coefficient, T_1 is the water spin-lattice relaxation time of tissue, and α is the arterial spin-labeling efficiency. Tissue T_1 of 1.5 seconds and α of 0.75 were measured using the method described elsewhere (Silva et al., 1995).

Lesion-volume determination

Lesion volumes (LV's) were derived using the CBF (57 ± 11% reduction, 0.30 ± 0.09 mL/g/min, n = 5, permanent occlusion) and the ADC (30 ± 2% reduction, 0.53 ± 0.03 × 10^{-3} mm^2/s) viability thresholds established previously (Shen et al., 2003). These thresholds were derived by setting a fixed value below which the lesion volumes of ADC or CBF maps at 3-hour were equal to the TTC infarct volume in the permanent occlusion group (Shen et al., 2003). In this study, previously determined *percent-change reduction* (not quantitative) *thresholds* were used to derive the ADC or CBF LV'S at each time points.

Pixel-by-Pixel analysis

For pixel-by-pixel analysis, only four anterior slices were used to minimize the effect of susceptibility distortion around the ear canals. Pixel-by-pixel CBF-ADC scatterplots were

analyzed at each time point. Four quadrants on the CBF-ADC scatterplots were operationally defined using the TTC-derived ADC and CBF thresholds determined previously (Shen et al., 2003): (1) the "normal" cluster, where both ADC and CBF were above their respective thresholds; (2) the "mismatch" cluster, where ADC was above but CBF was below their respective thresholds; (3) the "core" cluster, where both ADC and CBF were below their respective thresholds; and (4) "non-nourishing reperfusion zone" (also referred to as "zone 4"), where ADC was below but CBF was above their respective thresholds. For group averaging, the ADC and CBF of the left hemisphere (LH) at 60 minutes were normalized to a zero mean for each animal and the ADC and CBF of the right hemisphere (RH) were computed relative to the LH at each time point. Projection profiles of the ADC and CBF distributions were also analyzed. Tissue volumes, ADC and CBF of each cluster were evaluated at each time point.

Tissue volume, ADC and CBF of pixels that migrated to different zones

The effects of reperfusion on pixel dynamics in the CBF–ADC and image spaces were investigated. The 60-minute time point before reperfusion was used as a reference. The temporal evolution of the "core" and "mismatch" pixels, defined at 60 minutes before reperfusion, was evaluated as they migrated to different zones. Pixels that subsequently migrated into the normal zone, mismatch zone, core zone, or "non-nourishing reperfusion zone" were color-coded as green, yellow, red, or blue, respectively. These color pixels were mapped onto the image spaces for each time point. Tissue volumes, ADC and CBF values of the "mismatch", "core", and "non-nourishing reperfusion zone" pixels were quantified at 60 minutes and at 180 minutes for the same pixels. For comparison, similar analysis on the migrating pixels was performed on the permanent occlusion group (n = 11) (Shen et al., 2003).

Statistical analysis

A two-tail paired t-test was used for statistical comparison for all parametric values. A p value < 0.05 was considered statistically significant. All data in text were reported as mean ± SD and all error bars on graphs as standard errors of the means (SEM).

Results

Blood gases, measured once during surgery as well at approximately one and three hours after occlusion, were not statistically different from each other and were grouped together. All blood gases (pH = 7.37 ± 0.03, pCO_2 = 39 ± 6 mmHg, pO_2 = 83 ± 6 mmHg, O_2 saturation = 95 ± 2%), heart rate (370 ± 20 bpm), mean arterial blood pressure (102 ± 9 mmHg), rectal temperature (37.0 ± 0.5°C) were within normal physiological ranges.

Evolution of ischemic volume following 60-minute MCAO

Figure 1a-c shows a representative data set from an animal subjected to transient MCAO. The group-average CBF LV's at 30 minutes (250 ± 30 mm^3, mean ± SD, n = 6) and 60 minutes (240 ± 40 mm^3) were large and constant, whereas the ADC LV's grew slightly from 30 minutes (140 ± 20 mm^3) to 60 minutes (170 ± 20 mm^3). ADC LV's were statistically different from the CBF LV's at 30 and 60 minutes ($P < 0.05$). Following reperfusion, CBF LV's markedly decreased as most of the hypoperfused regions returned to normal although some pixels remained hypoperfused. ADC LV's also decreased immediately after reperfusion (104 ± 35 mm^3) and then increased slightly over time (110 ± 50 mm^3 at 3 hours), but did not reach the CBF-derived LV's at 60 minutes ($P < 0.05$). The mean TTC infract volume at 24 hours was 140 ± 30 mm^3, slightly higher than, but not statistically different from, the mean ADC LV's at 3 hours.

Pixel-by-pixel analysis of ischemic progression

Dynamics of ischemia progression in the CBF-ADC space and image space were analyzed on a pixel-by-pixel basis. Figure 2 shows representative CBF-ADC scatterplots from one animal subdivided into four quadrants, the boundaries of which were defined by the CBF (57 ±11% reduction) and ADC (30 ± 2% reduction) thresholds established previously (Shen et al., 2003). In the normal LH, there was a single cluster residing primarily in the normal zone. In the ischemic RH, pixels were distributed in multiple distinct zones (i.e., normal, mismatch, core and "zone 4") and they evolved dynamically with time. There was a large pixel population in the "mismatch" zone at 60 minutes prior to reperfusion that largely disappeared at 180 minutes (Fig. 2a).

To evaluate the effect of reperfusion in the spatial domain, evolution of different pixel populations in the CBF–ADF space were mapped onto the image space. The results from a representative animal are shown in Fig. 2b-c. After reperfusion, a substantial number of pixels in the core (red) zone at 60 minutes migrated to the normal (green) and the mismatch (yellow) zone, while some remained in the core zone (red) or moved to the non-nourishing reperfusion zone (blue) (Fig. 2b). Similarly, after reperfusion, a substantial number of mismatch (yellow) pixels at 60 minutes migrated to the normal zone, while some remained in the mismatch zone, but essentially none (<1%) migrated to the core or "non-nourishing reperfusion" zone (Fig. 2c).

The normalized group-average (n = 6) scatterplots for all time points and the temporal evolution of the tissue volumes of the four zones defined using the TTC-derived thresholds are shown in Fig. 3. For the group-average data, the appearance of the scatterplots for the normal left hemisphere, 60 minutes post MCAO, and 180 minutes post MCAO parallelled those of the corresponding plots shown in Fig. 2. Interestingly, upon reperfusion (i.e., at 70 minutes post MCAO), a transient hyperemic effect was apparent in the scatterplot, where a significant number of pixels with reduced ADC and CBF (i.e., in the core region) at 60 minutes of occlusion migrate into the "zone 4" region at 70 minutes. As time progressed from 90 to 180 minutes post-MCAO, the mean value of the CBF pixel population in the core and "zone 4" quadrants declined relative to that observed immediately upon reperfusion at 70 minutes post MCAO. The hyperemic effect is also apparent in the temporal evolution of the tissue volumes of the "zone 4" and core volumes in the graph. Notice the transient increase in the "zone 4" volume immediately upon reperfusion, which then declined over the ensuing 90 and 120 minutes time points (with a concomitant increase in core volume) as the hyperemia subsided.

Projection-profile analysis

Projection profiles of the group-average ADC and CBF distributions were analyzed (Fig. 4). The contralateral normal LH ADC had a uni-modal distribution with a mean of $0.75 \pm 0.08 \times 10^{-3}$ mm^2/s. The ipsilateral ischemic RH ADC distribution was bimodal with a distinct separation (a minimum) (Fig. 4a). The ADC bimodal minima ($ADC_{bimodal}$) were statistically different at 30 and 60 minutes before reperfusion (at − 21% percent-ADC-reduction, $0.59 \pm 0.01 \times 10^{-3}$ mm^2/s) and after reperfusion (at − 34% percent-ADC-reduction, $0.50 \pm 0.02 \times 10\text{-}^{3}$ mm^2/s). The corresponding $CBF_{ADC\text{-}bimodal}$ was obtained from the pixels that was within one standard deviation of the $ADC_{bimodal}$ and its value was 0.30 ± 0.01 mL/g/min before reperfusion.

The contralateral normal LH CBF had a distribution with a mean of 0.7 ± 0.2 mL/g/min. Unlike the ipsilateral ischemic RH ADC distributions, the CBF distributions of the RH were uni-modal (Fig. 4b). The mean RH CBF were markedly lower than the normal LH CBF before reperfusion and became similar after reperfusion, as expected.

Volume, ADC and CBF of migrating pixels

The fates of the core and mismatch pixels at 60 minutes were evaluated. Tissue volumes, ADC and CBF values of the core and mismatch pixels at 60 minutes were quantified on a pixel-by-pixel basis as ischemia progressed. Figure 5 shows the group-average tissue volumes (top row), ADC (middle row) and CBF (bottom row) values of the 60-minute core and mismatch pixels as they subsequently migrated to different zones at 180 minutes.

Core pixels—The volume of the core pixels (Fig. 5a) markedly decreased immediately after reperfusion and then increased slightly over time. At 180 minutes, 25% of the core pixels at 60 minutes migrated to the normal zone, 3% migrated to the mismatch zone, and 72% migrated to the core and "non-nourishing reperfusion" zones. At 60 minutes, the ADC values of the core pixels that subsequently migrated to the normal or mismatch zones were slightly higher than those that subsequently migrated to the "non-nourishing reperfusion zone" or remained in the core zone. At 180 minutes, the ADC of these same pixels that subsequently migrated to the normal or mismatch zone were normal, whereas those that migrated to "non-nourishing reperfusion zone" or remained in the core zone were abnormal. Similarly, CBF of all pixels classified as core at 60 minutes were low. At 180 minutes, only the CBF of the same pixels that eventually migrated to the normal zone or "non-nourishing reperfusion zone" returned to normal.

Mismatch pixels—After reperfusion, the mismatch volume decreased markedly with majority of these pixels (83%) migrating to the normal zone (Fig. 5b). At 60 minutes, the ADC and CBF of the mismatch pixels that subsequently migrated to the normal region or remained in the mismatch zone were higher than those that migrated to the core or "non-nourishing reperfusion" zone ($P < 0.05$). At 180 minutes, only the ADC of these same pixels that migrated to the normal zone or remained in the mismatch zone did not markedly decrease, and only the CBF of these same pixels that migrated to the normal zone or "zone 4" returned to normal.

Mismatch pixels (permanent MCAO, n = 11)—A similar analysis was performed on the permanent occlusion group (Shen et al., 2003) for comparison. Since essentially none (<4%) of the 30-minutes "core" pixels migrated to other zones and the number of "non-nourishing reperfusion zone" pixels was negligible (<5%), they were not analyzed. The mismatch volume (Fig. 5c) decreased as ischemia progressed with 59% migrating to the core zone and 26% remaining in the mismatch zone at 180 minutes. At 30 minutes, ADC of the mismatch pixels that subsequently migrated to the normal zone were higher ($P < 0.05$) than those remained in the mismatch zone, which in turn were higher than those that migrated to the core zone ($P < 0.05$). At 180 minutes, only the ADC of these same pixels that migrated to the normal or remained in the mismatch zone did not markedly decrease, and only the CBF of these same pixels that migrated to the normal zone returned to normal.

Discussion

The major results of this study can be summarized as follows. (1) The "lesion" volumes of transient focal ischemic injury could be quantified and reperfusion salvaged substantial amount of potentially ischemic tissues. (2) Pixel-by-pixel analysis of the ADC and CBF tissue characteristics based on four pixel populations (defined with respect to the fixed ADC and CBF thresholds) made possible the quantitative evaluation of tissue volumes, ADC and CBF of different tissue types as they were modulated by reperfusion. (3) Pixel distributions showed bimodal ADC, but uni-modal CBF, distributions. The $ADC_{bimodal}$ minimum and the corresponding $CBF_{ADC\text{-}bimodal}$ were similar to the histology-derived thresholds. (4) Pixels from different population zones within the CBF–ADC space could be mapped onto the image space, thereby making it possible to evaluate the spatiotemporal ischemic progression and the

reperfusion effects on a pixel-by-pixel basis. (5) Some core and mismatch pixels were salvaged by reperfusion. ADC and CBF of "at risk" tissues that were subsequently salvaged were higher than those that subsequently became infarcted and the ADC and CBF of the salvaged tissues were indeed normal.

This study relied heavily on the accuracy of CBF measurements. Although consistent with many established invasive techniques, the accuracy of this CBF technique could be subjected to errors arising from magnetization-transfer (Silva et al., 1999; Duong et al., 2000), transit-time (Calamante et al., 1996; Zhou et al., 2001), and water-exchange (Silva et al., 1997a; Zhou et al., 2001; Parkes and Tofts, 2002) effects. Magnetization-transfer effect was not an issue with the actively decoupled two-coil system (Silva et al., 1999; Duong et al., 2000). Transit-time and water-exchange effects have been demonstrated to be small (Silva et al., 1997a; Zhou et al., 2001; Parkes and Tofts, 2002) and were unlikely to alter the overall conclusions of this study. Since CBF quantification involved subtraction of labeled and non-labeled images, as well as division of a combination of those signals, the calculated CBF could become slightly negative due to noise if the true tissue CBF is zero or close to zero (Fig. 2a). The few pixels that showed negative CBF values were within measurement uncertainties on the pixel-by-pixel basis.

The premise of the pixel-by-pixel analysis approach used herein was based on the notion that the different biologically relevant pixel populations could be approximated using fixed histology-derived ADC and CBF viability thresholds (Shen et al., 2003). The use of fixed viability CBF and ADC thresholds to delineate ischemic lesions across different time points had been suggested previously, although they were correlated with different post-mortem histological, biochemical or autoradiographic techniques. Crockard et al. used a hydrogen-clearance-electrode technique and reported a CBF threshold of 0.2 mL/g/min that best correlated with the loss of high-energy phosphates (Crockard et al., 1987). Naritomi et al. used ^{14}C-iodoantipyrine autoradiography and reported a CBF threshold of 0.12 to 0.20 mL/g/min that best correlated with the loss of sodium-ATPase pump failure (Naritomi et al., 1988). Hoehn-Berlage et al. used ^{14}C-iodoantipyrine autoradiography and derived a CBF threshold of 0.2 mL/g/min based on correlation with loss of energy metabolism (ATP depletion stained by post mortem bioluminescent technique) (Hoehn-Berlage et al., 1995). Busza et al. used hydrogen-clearance-electrode technique and derived a threshold of 0.15 to 0.20 mL/g/min that correlated with the onset of DWI contrast in a gerbil four-vessel-occlusion stroke model (Busza et al., 1992). Our CBF viability threshold was higher than these thresholds for energy failure. Kohno et al. used ^{14}C-iodoantipyrine autoradiography and reported a CBF threshold of 0.31 ± 0.11 mL/g/min, which correlated with the onset of reduced glucose metabolism and lactate acidosis but before energetic failure (Kohno et al., 1995). Belayev et al. and Zhao et al. used ^{14}C-iodoantipyrine autoradiography and derived upper CBF limits for the ischemic core and the penumbra of 0.24 and 0.47 mL/g/min, respectively; the average penumbral CBF threshold was reported to be 0.3 mL/g/min (Belayev et al., 1997; Zhao et al., 1997). While these critical thresholds derived using different post-mortem correlation techniques are expected to be slightly different from each other, our TTC-derived thresholds were most consistent with onset of reduced glucose metabolism and lactate acidosis (Kohno et al., 1995), and the penumbral CBF threshold (Belayev et al., 1997; Zhao et al., 1997). These comparisons suggest that "penumbra" is destined to become infarcted if left untreated and consequently our TTC-derived thresholds predicted infarction at 24 hours.

In regards to ADC thresholds in animal model, the literature is relatively sparse. Hoehn-Berlage, Olah and colleagues (Olah et al., 2001; Hoehn-Berlage et al., 1995) established a minimum ADC threshold by correlating with metabolic energy failure (ATP depletion stained by a post mortem bioluminescent technique). They reported that an ADC threshold of 77% of normal was a good estimate at all time points during the MCAO period as well as the early

phase of reperfusion. Despite different methodologies and errors associated with different cross-modality comparisons, our ADC threshold of 70% of normal was in reasonable agreement.

These comparisons clearly suggest that different critical thresholds exist for different biological events following ischemia and that these thresholds are dependent on animal models, anesthetics used, duration and/or severity of ischemic injury, and the accuracy of cross-modality comparision. Nevertheless, these viability thresholds are in principle applicable at all MCAO time points and during subsequent recirculation, and these thresholds "predict" infarction at 24 hours if the ischemic injury was left untreated (Shen et al., 2003). The CBF threshold was further justified (Shen et al., 2003) since the CBF–derived lesion volume in the permanent occlusion group remained stable over the 3-hour imaging period and the TTC-derived ADC threshold is consistent with the natural separation in the ADC profile ($ADC_{bimodal}$). These observations together support the premise of using fixed TTC-derived thresholds to approximate different clusters of tissue fate. It should be noted that percent reduction of the viability ADC and CBF thresholds were used, instead of the absolute quantitative ADC and CBF thresholds. Since the experimental conditions between the current study and the previous study (Shen et al., 2003) from which the viability thresholds were derived were essentially identical, either choice yielded similar lesion-volume results. The quantitative CBF threshold, however, is likely to be more universal (across laboratories) because it reflects the absolute CBF value below which tissues could become infarcted. The relative CBF, on the other hand, could be dependent on other factors. For example, different anesthetics used could result in slightly different relative CBF threshold. Similar comments can be made for the ADC threshold, although the effect is likely to be less bacause ADC is less dependent on anesthetics and other factors (assuming temperature is kept relatively constant).

Effects of Reperfusion on Lesion Volumes: Reperfusion salvaged a substantial amount of at-risk tissues. Our results are consistent with those reported previously (Dardzinski et al., 1993; Minematsu et al., 1993; Li et al., 1999; Li et al., 2000a; Li et al., 2000b; Kidwell et al., 2002). However, previous studies did not resolve tissues on a pixel-by-pixel basis or quantitatively evaluate their fates, tissue volume, ADC and CBF values as they evolved in the image and CBF-ADC spaces. We hypothesized that the combined ADC and CBF tissue characteristics could be used to characterize the ischemic tissue fates after reperfusion during the acute phase. *Pixel-by-pixel* analysis was performed to test this hypothesis by evaluating the ADC and CBF values before and after they migrated to various zones. The "core" and "mismatch" pixels at 60 minutes were most dynamic. Using this analysis approach, it was determined that the salvaged tissues arose from both the mismatch and core zones. Specifically, at 180 minutes following reperfusion, 28% of the core pixels at 60 minutes and 90% of the mismatch pixels at 60 minutes returned to normal based on tissue ADC and CBF characteristics. ADC and CBF of the salvaged tissues did indeed return to normal whereas those of the non-salvaged tissue did not. Since the 180-minute ADC LV's reflected tissue to a great extent infarction at 24 hours (although there was some delayed cell death), we concluded these tissues were predominantly salvaged by reperfusion. Without reperfusion (permanent occlusion group), 0% of the "core" and 13% of the "mismatch" pixels did not go onto infarct. Salvaging "core" pixels suggested that ADC reduction was not synonymous with irreversible injury. Duration of exposure to reduced ADC was likely critical. The ADC decline in turn is expected to be dependent on the degree and duration of CBF deficit, among other factors. Interestingly, some tissues with ADC returning to normal immediately after reperfusion showed subsequent ADC reduction, consistent with the secondary ADC decline observed previously using ROI volumetric analysis (Li et al., 2000b). In summary, our analysis approach demonstrated that ischemic tissue fates could be systematically characterized in both image and CBF-ADC spaces on a pixel-by-pixel basis.

Effects of Reactive Hyperemia: A transient hyperemic effect (i.e., at the 70-minute time point) was observed, consistent with observations by several groups during the first hour of reflow following transient focal cerebral ischemia in animal models (De Crespigny et al., 1992; Hamberg et al., 1996; Olah et al., 2001). Hyperemia could affect tissue-volume quantitation of various zones as defined by the fixed CBF threshold. The transient increased blood flow due to hyperemia resulted in a temporary CBF increase that exceeded the CBF-reduction threshold for some of the pixels used to calculate the zone-derived tissue volume. Consequently, hyperemia resulted in a decrease in the tissue volume for those zones with relatively lower CBF (e.g., core and mismatch) with a concomitant increase in lesion volume for those zones with a relatively higher CBF (e.g., normal and "zone 4"). However, the hyperemic effect appeared relatively small and transient. Detailed analysis of the hyperemic effects on a pixel-by-pixel basis is beyond the scope of this work.

Bimodal ADC Minimum: In contrast to the CBF distribution, a bimodal ADC minimum ($ADC_{bimodal}$) was observed. The $ADC_{bimodal}$ before reperfusion was slightly higher than that after reperfusion (Fig. 4), suggesting that the underpinning biophysical mechanism(s) of ischemia-induced ADC decline might be different. For example, reperfusion could lead to secondary effects such as vasogenic edema (Rosenberg, 1999), which could account for further ADC reduction, although other factors associated with reperfusion injuries (Hallenbeck and Dutka, 1990) could also play a role.

The important observations regarding the ADC bimodal minimum are: 1) the fact that a separation (minimum) exists, instead of a continuous distribution; 2) the right-hand-mode of the ipsilateral ischemic RH ADC distribution was normal and time-invariant; and 3) the $ADC_{bimodal}$ minima were similar to the TTC-derived threshold and relatively time invariant. These observations could have major implications, as they suggests that there is a critical (distinct) ADC value below which there are definitive changes in tissue biophysical properties, which is likely to correlate with a major cellular event(s) in the cascades of ischemic injury. The ADC bimodal minimum is likely to be well-defined; the loss of definition is likely due to partial-volume effects arising from limited spatial resolution as well as scattering from inter-subject averaging. Imaging at a higher spatial resolution and analysis of individual animals could directly test this hypothesis. It is further postulated that the ADC bimodal minimum ($0.59 \pm 0.01 \times 10^{-3}$ mm^2/s) is a naturally occurring threshold that could be used to approximate the "viability threshold" without the need for histological correlation.

The $CBF_{ADC\text{-}bimodal}$ minimum associated with the $ADC_{bimodal}$ minimum ranged from 0.30 to 0.35 mL/g/min, similar to the histology-derived viability threshold. The slight differences between the histology-derived viability thresholds and the ADC bimodal minima could be due to errors in correlating histology with MR–defined lesion volumes. Surprisingly, the $CBF_{ADC\text{-}bimodal}$ was similar to the CBF threshold of lactate acidosis, reduced glucose metabolism and the penumbral CBF threshold (~0.3 mL/g/min) but significantly higher than the CBF threshold (~0.2 mL/g/min) for energetic failure and loss of cell-volume homeostasis. Further studies are warranted to validate whether the ADC bimodal minima are the same as the ADC and CBF viability thresholds and to investigate the under lying biophysical and biological event(s) associated with the ADC bimodal minima. If indeed the $ADC_{bimodal}$ and its corresponding CBF approximated the viability thresholds, they could have important clinical implications as histological analysis is generally not possible in clinical settings.

Conclusion

This study established a quantitative imaging and an analysis protocol to evaluate, on a pixel-by-pixel basis, the spatio-temporal evolution of ischemic brain injury in a reperfusion rat stroke model. Tissue fates at different time points could be identified based on diffusion-perfusion

tissue properties and mapped onto the image spaces. Tissue volumes, ADC and CBF values that were subsequently salvaged or inevitably become infarcted could be quantitatively evaluated on a pixel-by-pixel basis. This analysis approach is expected to provide a powerful tool to evaluate drug efficacy, and potentially offer a means to make statistical prediction of tissue fates associated with ischemic brain injury.

Acknowledgments

The authors acknowledge Xiangjun Meng for technical assistance. This work was supported in part by the American Heart Association and the Whitaker Foundation.

This work was supported in part by a Biomedical Engineering grant from the Whitaker Foundation and a Scientist Development Grant from the American Heart Association (TQD).

References

Albers GW. Expanding the window for thrombolytic therapy in acute stroke: The potential role of acute MRI for patient selection. Stroke 1999;30:2230–2237. [PubMed: 10512933]

Astrup J, Symon L, Siesjo BK. Thresholds in cerebral ischemia: the ischemic penumbra. Stroke 1981;12:723–725. [PubMed: 6272455]

Back T, Hoehn-Berlage M, Kohno K, Hossmann KA. Diffusion nuclear magnetic resonance imaging in experimental stroke correlation with cerebral metabolites. Stroke 1994;25:494–500. [PubMed: 8303762]

Baird AE, Benfield A, Schlaug G, Siewert B, Lovblad KO, Edelman RR, Warach S. Enlargement of human cerebral ischemic lesion volumes measured by diffusion-weighted magnetic resonance imaging. Ann Neurol 1997;41:581–589. [PubMed: 9153519]

Belayev L, Zhao W, Busto R, Ginsberg MD. Transient middle cerebral artery occlusion by intraluminal suture: I. Three-dimensional autoradiographic image-analysis of local cerebral glucose metabolism-blood flow interrelationships during ischemia and early recirculation. J Cereb Blood Flow and Metab 1997;17:1266–1280. [PubMed: 9397026]

Busza AL, Allen KL, King MD, van Bruggen N, Williams SR, Gadian DG. Diffusion-weighted imaging studies of cerebral ischemia in gerbils: Potential relevance to energy failure. Stroke 1992;23:1602–1612. [PubMed: 1440708]

Calamante F, Williams SR, van Bruggen N, Kwong KK, Turner R. A model for quantification of perfusion in pulsed labeling techniques. NMR in Biomed 1996;9:79–83.

Carano RA, Li F, Irie K, Helmer KG, Silva MD, Fisher M, Sotak CH. Multispectral analysis of the temporal evolution of cerebral ischemia in the rat brain. J Magn Reson Imag 2000;12:842–858.

Crockard HA, Gadian DG, Frackowiak RS, Proctor E, Allen K, Williams SR, Russell RW. Acute cerebral ischemia: concurrent changes in cerebral blood flow, energy metabolites, pH, and lactate measured with hydrogen clearance and 31P and 1H nuclear magnetic resonance spectroscopy. II. Changes during ischemia. J Cereb Blood Flow and Metab 1987;7:394–402. [PubMed: 3611203]

Dardzinski BJ, Sotak CH, Fisher M, Hasegawa Y, Li F, Minematsu K. Apparent diffusion coefficient mapping of experimental focal cerebral ischemia using diffusion-weighted echo-planar imaging. Magn Reson Med 1993;30:318–325. [PubMed: 8412602]

De Crespigny AJ, Wendland MF, Derugin N, Kozniewska E, Moseley ME. Real-time observation of transient focal ischemia and hyperemia in cat brain. Magn Reson Med 1992;27:391–397. [PubMed: 1461120]

Duong TQ, Silva AC, Lee SP, Kim SG. Functional MRI of calcium-dependent synaptic activity: cross correlation with CBF and BOLD measurements. Magn Reson Med 2000;43:383–392. [PubMed: 10725881]

Fisher M, Albers GW. Applications of diffusion-perfusion magnetic resonance imaging in acute human stroke. Neurology 1999;52:1750–1756. [PubMed: 10371519]

Franke C, Brinker G, Pillekamp F, Hoehn M. Probability of metabolic tissue recovery after thrombolytic treatment of experimental stroke: a magnetic resonance spectroscopic imaging study in rat brain. J Cereb Blood Flow and Metab 2000;20:583–591. [PubMed: 10724122]

Hallenbeck JM, Dutka AJ. Background review and current concepts of reperfusion injury. Arch Neurol 1990;47:1245–1254. [PubMed: 2241624]

Hamberg LM, Boccalini P, Stranjalis G, Hunter GJ, Huang Z, Halpern E, Weisskoff RM, Moskowitz MA, Rosen BR. Continuous assessment of relative cerebral blood volume in transient ischemia using steady-state susceptibility-contrast MRI. Magn Reson Med 1996;35:168–173. [PubMed: 8622580]

Hoehn-Berlage M, Norris DG, Kohno K, Mies G, Leibfritz D, Hossmann KA. Evolution of regional changes in apparent diffusion coefficient during focal ischemia of rat brain: the relationship of quantitative diffusion NMR imaging to reduction in cerebral blood flow and metabolic disturbances. J Cereb Blood Flow Metab 1995;15:1002–1011. [PubMed: 7593332]

Karonen JO, Vanninen RL, Liu Y, Ostergaard L, Kuikka JT, Nuutinen J, Vanninen EJ, Partanen PL, Vainio PA, Korhonen K, Perkio J, Roivainen R, Sivenius J, Aronen HJ. Combined diffusion and perfusion MRI with correlation to single-photon emission CT in acute ischemic stroke. Ischemic penumbra predicts infarct growth. Stroke 1999;30:1583–1590. [PubMed: 10436105]

Kaufmann AM, Firlik AD, Fukui MB, Weshsler LR, Jungries CA, Yonas H. Ischemic core and penumbra in human stroke. Stroke 1999;30:93–99. [PubMed: 9880395]

Kidwell CS, Saver JL, Mattiello J, Starkman S, Vinuela F, Duckwiler G, Gobin P, Jahan R, Vespa P, Kalafut M, Alger JR. Thrombolytic reversal of acute human cerebral ischemia injury shown by diffusion/perfusion magnetic resonance imaging. Ann Neurol 2000;47:462–469. [PubMed: 10762157]

Kidwell CS, Saver JL, Starkman S, Duckweiler G, Jahan R, Vespa JP, Villablanca JP, Liebeskind DS, Gobin YP, Vinuela F, Alger JR. Late secondary ischemic injury in patients receiving intra-arterial thrombolysis. Ann Neurol 2002;52:698–703. [PubMed: 12447922]

Kohno K, Hoehn-Berlage M, Mies G, Back T, Hossmann KA. Relationship between diffusion-weighted MR images, cerebral blood flow, and energy state in experimental brain infarction. Magn Reson Imag 1995;13:73–80.

Li F, Han SS, Tatlisumak T, Liu KF, Garcia JH, Sotak CH, Fisher M. Reversal of acute apparent diffusion coefficient abnormalities and delayed neuronal death following transient focal cerebral ischemia in rats: correlation with histopathology. Ann Neurol 1999;46:333–342. [PubMed: 10482264]

Li F, Liu KF, Silva MD, Omae T, Sotak CH, Fenstermacher JD, Fisher M. Transient and permanent resolution of ischemic lesions on diffusion-weighted imaging after brief periods of focal ischemia in rats. Stroke 2000a;31:946–954. [PubMed: 10754004]

Li F, Silva MD, Liu KF, Helmer KG, Omae T, Fenstermacher JD, Sotak CH, Fisher M. Secondary decline in apparent diffusion coefficient and neurological outcomes after a short period of focal brain ischemia in rats. Ann Neurol 2000b;48:236–244. [PubMed: 10939575]

Lythgoe MF, Busza AL, Calamante F, Sotak CH, King MD, Bingham AC, Williams SR, Gadian DG. Effects of diffusion anisotropy on lesion delineation in a rat model of cerebral ischemia. Magn Reson Med 1997;38:662–668. [PubMed: 9324334]

Lythgoe MF, Williams SR, Busza AL, Wiebe L, McEwan AJ, Gadian DG, Gordon I. The relationship between magnetic resonance diffusion imaging and autoradiographic markers of cerebral blood flow and hypoxia in an animal stroke model. Magn Reson Imag 1999;41:706–714.

Minematsu K, Fisher M, Li L, Sotak CH. Diffusion and perfusion magnetic resonance imaging studies to evaluate a noncompetitive N-Methyl-D-aspartate antagonist and reperfusion in experimental stroke in rats. Stroke 1993;24:2074–2081. [PubMed: 8248990]

Moseley ME, Cohen Y, Mintorovitch J, Chileuitt L, Shimizu H, Kucharczyk J, Wendland MF, Weinstein PR. Early detection of regional cerebral ischemia in cats: comparison of diffusion- and T2-weighted MRI and spectroscopy. Magn Reson Med 1990;14:330–346. [PubMed: 2345513]

Naritomi H, Sasaki M, Kanashiro M. Flow thresholds for cerebral energy disturbance and Na+ pump failure as studied by *in vivo* 31P and 23Na nuclear magnetic resonance spectroscopy. J Cereb Blood Flow Metab 1988;8:16–23. [PubMed: 2448321]

Neumann–Haefelin T, Wittsack HJ, Wenserski F, Siebler M, Seitz RJ, Modder U, Freund HJ. Diffusion - and perfusion-weighted MRI. The DWI/PWI mismatch region in acute stroke. Stroke 1999;30:1591–1597. [PubMed: 10436106]

Olah L, Wecker S, Hoehn M. Relation of apparent diffusion coefficient changes and metabolic disturbance after 1 hour of focal cerebral ischemia and at different reperfusion phases in rats. J Cereb Blood Flow and Metab 2001;21:430–439. [PubMed: 11323529]

Parkes LM, Tofts PS. Improved accuracy of human cerebral blood perfusion measurements using arterial spin labeling: Accounting for capillary water permeability. Magn Reson Med 2002;48:27–41. [PubMed: 12111929]

Rohl L, Ostergaard L, Simonsen CZ, Vestergaard-Poulsen P, Andersen G, Sakoh M, Le Bihan D, Gyldensted C. Viability thresholds of ischemic penumbra of hyperacute stroke defined by perfusion-weighted MRI and apparent diffusion coefficient. Stroke 2001;32:1140–1146. [PubMed: 11340223]

Rosenberg GA. Ischemic brain edema. Prog Cardivasc Dis 1999;42:209–216.

Schlaug G, Benfield A, Baird AE, Siewert B, Lovblad KO, Parker RA, Edelman RR, Warach S. The ischemic penumbra: operationally defined by diffusion and perfusion MRI. Neurology 1999;53:1528–1537. [PubMed: 10534263]

Shen Q, Meng X, Fisher M, Sotak CH, Duong TQ. Pixel-by-pixel spatiotemporal progression of focal ischemia derived using quantitative perfusion and diffusion imaging. J Cereb Blood Flow Metab 2003;23:1479–1488. [PubMed: 14663344]

Silva AC, Zhang W, Williams DS, Koretsky AP. Multi-slice MRI of rat brain perfusion during amphetamine stimulation using arterial spin labeling. Magn Reson Med 1995;33:209–214. [PubMed: 7707911]

Silva AC, Williams DS, Koretsky AP. Evidence for the exchange of arterial spin-labeled water with tissue water in rat brain from diffusion-sensitized measurements of perfusion. Magn Reson Med 1997a; 38:232–237. [PubMed: 9256102]

Silva AC, Zhang W, Williams DS, Koretsky AP. Estimation of water extraction fractions in rat brain using magnetic resonance measurement of perfusion with arterial spin labeling. Magn Reson Med 1997b;37:58–68. [PubMed: 8978633]

Silva AC, Lee SP, Yang C, Iadecola C, Kim SG. Simultaneous BOLD and perfusion functional MRI during forepaw stimulation in rats. J Cereb Blood Flow Metab 1999;19:871–879. [PubMed: 10458594]

Stejskal EO, Tanner JE. Spin diffusion measurements: Spin echoes in the presence of a time-dependent field gradient. J Chem Physics 1965;42:288–292.

Strupp JP. Stimulate: A GUI based fMRI analysis software package. NeuroImage 1996;3:S607.

Tatlisumak T, Carano RA, Takano K, Opgenorth T, Sotak CH, Fisher M. A novel endothelin antagonist, A-127722, attenuates ischemic lesion size in rats with temporal middle cerebral artery occlusion: a diffusion and perfusion MRI study. Stroke 1998;29:850–858. [PubMed: 9550522]

Williams DS, Detre JA, Leigh JS, Koretsky AP. Magnetic resonance imaging of perfusion using spin inversion of arterial water. Proc Natl Acad Sci USA 1992;89:212–216. [PubMed: 1729691]

Wu O, Koroshetz WJ, Ostergard L, Buonanno FS, Copen W, Gonzales R, Rordorf G, Rosen BR, Schwamm LH, Weisskoff RM, Sorensen AG. Predicting tissue outcome in acute human cerebral ischemia using combined diffusion- and perfusion-weighted MR imaging. Stroke 2001;32:933–942. [PubMed: 11283394]

Zhao W, Belayev L, Ginsberg MD. Transient middle cerebral artery occlusion by intraluminal suture: II. Neurological deficits, and pixel-based correlation of histopathology with local blood flow and glucose utilization. J Cereb Blood Flow and Metab 1997;17:1281–1290. [PubMed: 9397027]

Zhou J, Wilson DA, Ulatowski JA, Traystman RJ, van Zijl PC. Two-compartment exchange model for perfusion quantification using arterial spin tagging. J Cereb Blood Flow Metab 2001;21:440–455. [PubMed: 11323530]

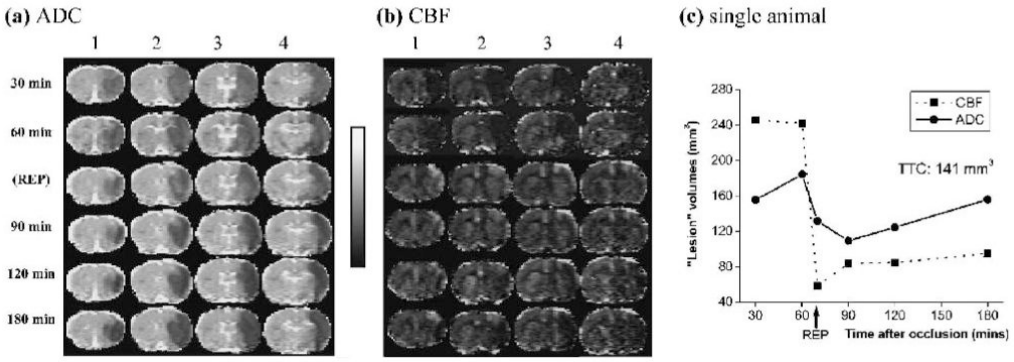

FIG. 1.

Representative (a) ADC and (b) CBF maps from one animal. Four of seven multislice ADC_{av} and CBF maps are shown at 30, 60, immediately after reperfusion (labeled as REP at 70 minutes), 90, 120, and 180 minutes post-ischemia. The TTC infarct volume at 24 hours for this animal was 141 mm^3. The grayscale bar indicates ADC ranges from 0 to 0.001 mm^2/s and CBF ranges from - 1 to 2 mL/g/min. (c) Temporal progression of ADC- and CBF-defined lesion volumes determined by using the group-average viability thresholds (57% and 30% reduction for CBF and ADC thresholds, respectively), as previously determined (Shen et al., 2003).

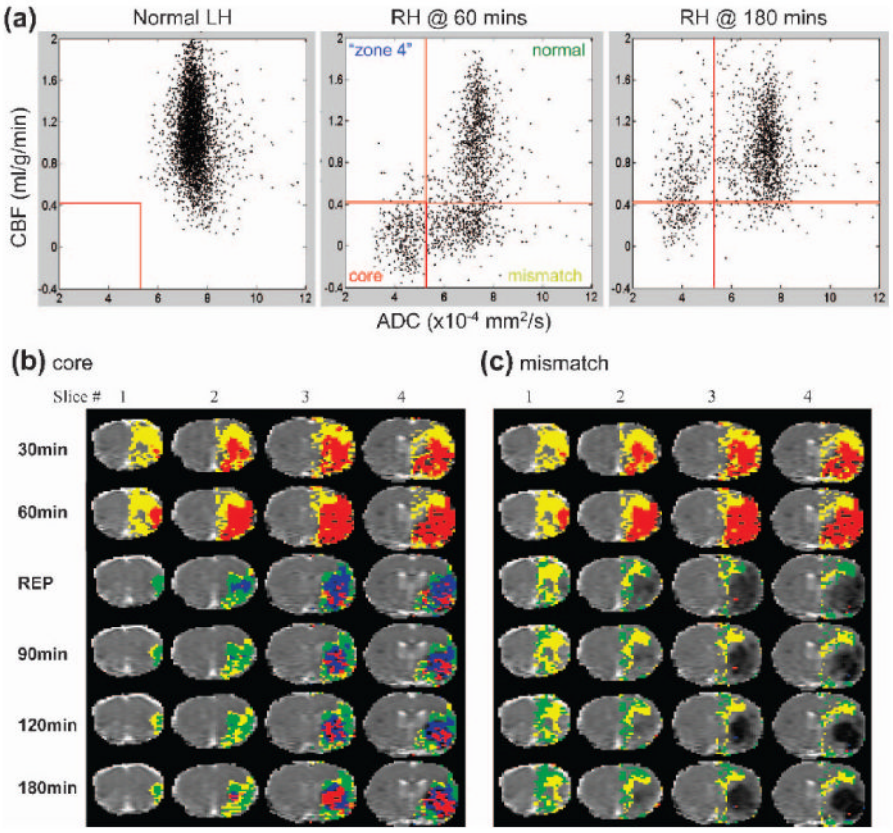

FIG. 2.

(a) CBF-ADC scatterplots of the contralateral normal left hemisphere and ipsilateral ischemic right hemisphere at 60 and 180 minutes. The dotted red lines indicate the group-average CBF and ADC viability thresholds (57 ± 11% reduction and 30 ± 2% reduction, respectively, as previously determined (Shen et al., 2003)), which divide the scatterplots into four zones, namely: the normal, mismatch, core zone and "non-nourishing reperfusion zone" (or "zone" 4). CBF axis range: - 0.4 to 2 mL/g/min; ADC axis range: 2 to 12 × 10^{-4} mm^2/s. The spatial evolution of (b) "core" and (c) "mismatch" pixels defined at 60 minutes from a representative animal. The 60-minute time point before reperfusion was used as a reference to evaluate the effect of reperfusion. Pixels that migrated into different zones after reperfusion were color-coded and mapped onto the image spaces. Pixels that belonged to the normal zone are displayed in green, mismatch zone in yellow, core zone in red, and "non-nourishing reperfusion zone" in blue.

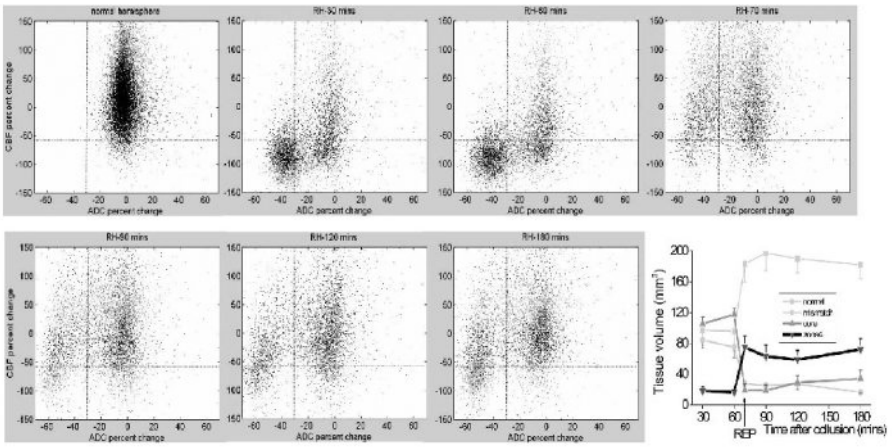

FIG. 3.

Normalized pixel-by-pixel CBF–ADC scatterplots from all animals (n = 6). Scatterplots were obtained from the normal left hemisphere (for all time points except 70 minutes) and from ischemic right hemisphere at 30 minutes, 60 minutes, immediately after reperfusion (labeled as REP at 70 minutes), 90 minutes, 120 minutes, and 180 minutes post-occlusion. Superimposed as dotted lines on the scatterplots are the TTC-derived CBF and ADC thresholds as previously determined (Shen et al., 2003), which divide the scatterplots into four zones, namely: the normal, mismatch, core zone and “non-nourishing reperfusion zone”. Values reported in the text were obtained with a limit of ± 150% of normal CBF and ± 70% of normal ADC as displayed; pixels outside of these limits were negligible (< 5%) and mostly arose from noise and/or pixels at the edge of the brain. The plot summarizes the temporal evolution of the tissue volumes of the four zones defined using the TTC-derived thresholds. Error bars are SEM.

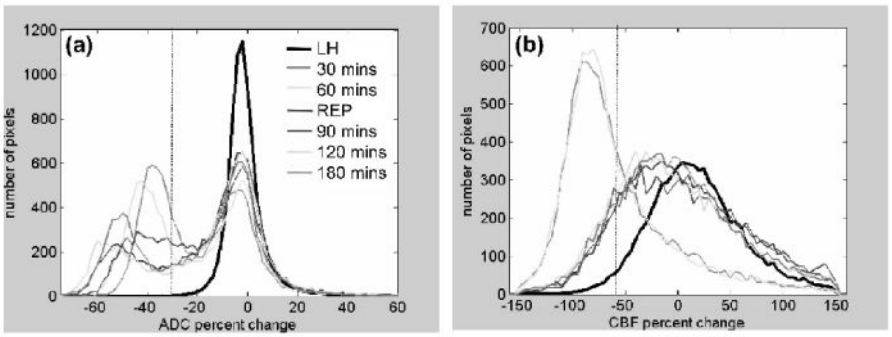

FIG. 4.

(a) ADC and (b) CBF projection profiles from the scatterplots in Fig. 3 (n = 6) as a function of time (30 and 60 minutes, pre-reperfusion; 70, 90, 120, and 180 minute, post-reperfusion). Pixel distributions were plotted for the entire left hemisphere (for the five time points, excluding 70 minutes, and divided by five for displaying on the same scale). Pixel distributions were plotted for the entire right hemisphere for each time point. The ADC distribution was bimodal but the CBF was uni-modal. Superimposed on these distributions are the vertical dotted lines indicating TTC-derived ADC (- 30%) or CBF (- 57%) viability thresholds as previously determined (Shen et al., 2003).

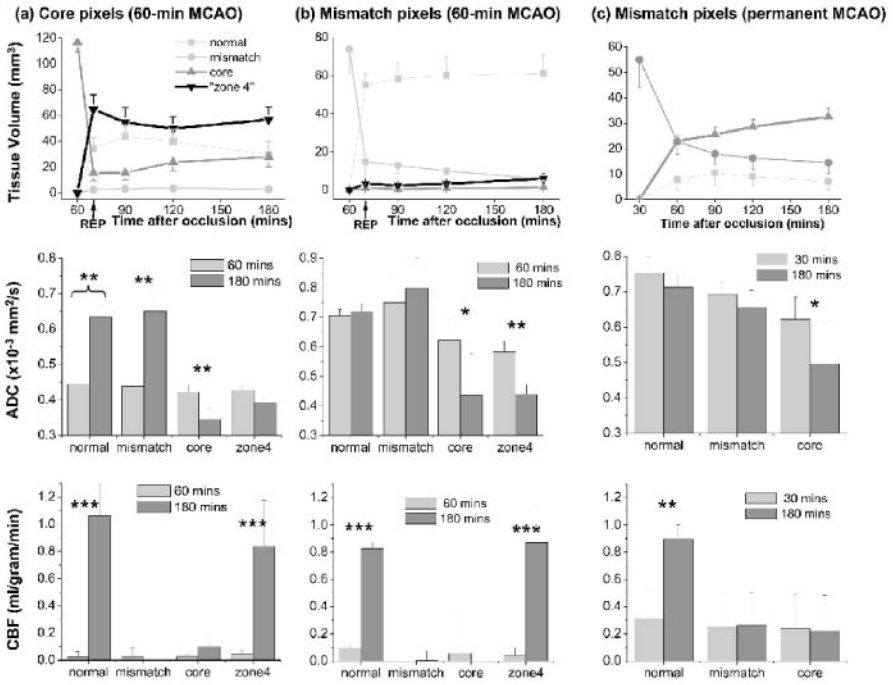

FIG. 5.

Group-average evolutions of tissue volumes (top row), ADC (middle row) and CBF (bottom row) values before and after migration to different zones for (a) core pixels (n = 6, 60-minute MCAO), (b) mismatch pixels (n = 6, 60-minute occlusion), and (c) mismatch pixels (n = 11, permanent occlusion). Comparison was made relative to 60 minutes. As ischemia evolved, these pixels migrated to different zones. The ADC (middle row) and CBF (bottom row) before (60 minutes) and after (180 minutes) reperfusion were quantified. Pixels that migrated into the normal zone are displayed as very light gray, mismatch zone as light gray, core zone as dark gray, and "non-nourishing reperfusion zone" ("zone 4") as black. "Zone 4" pixels in (c) were negligible and were not plotted. Error bars are SEM. * $P < 0.05$, ** $P < 0.01$, *** $P < 0.001$.